Journal of Materials Science: Materials in Electronics (2018) 29:16581–16589
https://doi.org/10.1007/s10854-018-9751-3

Dielectric property and self-repairing capability of silicon and titanium co-doped amorphous alumina thin films prepared by sol–gel technology

Qian Feng[1] · Manwen Yao[1] · Zhen Su[1] · Xi Yao[1]

Received: 26 May 2018 / Accepted: 25 July 2018 / Published online: 16 August 2018
© Springer Science+Business Media, LLC, part of Springer Nature 2018

Abstract

In this article, $(Al_{1-0.02-x}Si_{0.02}Ti_x)_2O_y$ (x = 0.2, 0.9 and 2%) thin films were prepared on $Pt/Ti/SiO_2/Si$ substrates using sol–gel technique. The dielectric properties of undoped and Si–Ti co-doped Al_2O_3 thin films were investigated. The leakage current of $(Al_{0.971}Si_{0.02}Ti_{0.009})_2O_y$ thin film is reduced by 2 orders of magnitude compared with Al_2O_3 film. Meanwhile, the modified sample exhibits the ultrahigh energy density of 14.01 J/cm^3 under the breakdown strength of 647 MV/m, which is an enhancement of 11.26 J/cm^3 over that of the undoped Al_2O_3 film. The improvement of dielectric properties is ascribed to the forming of Al–O–Si, Al–O–Ti bonds and the anodic oxidation of Ti^{3+}, which could strengthen the stability of Al_2O_3 structure and self-repair the defects of the films under applied electric field. Another reason is that cation vacancies generated by Si–Ti co-doping could effectively prevent the formation of oxygen vacancies and decrease the breakdown probability of the films. This work provides a promising route to dielectric thin films materials for electrical energy storage applications.

1 Introduction

Green energy has become one of the most significant issues in the twenty-first century because of the vast consumption of fossil fuels and the worsening of environmental pollution [1]. Dielectric capacitor is one of the major circuit components in electronics and also widely recognized as a kind of traditional electric energy storage devices. Electronic circuits are moving toward miniaturization, portability, high reliability and large-scale integration, so that dielectric materials with high energy storage density are intensively desired [2]. The energy storage density (U_e) of dielectric capacitors is given by

$$U_e = \int EdD \tag{1}$$

and for simple linear dielectric materials, it can be defined as

$$U_e = 1/2\varepsilon_0\varepsilon_r E^2 \tag{2}$$

where ε_0 is the vacuum dielectric constant (8.8542×10^{-12} F/m), ε_r is the relative dielectric constant, and E is the dielectric breakdown strength [3, 4]. In order to increase the energy storage density, one can increase either the dielectric constant or breakdown strength. From the first glance, it seems that enhancing the breakdown strength is more attractive because the energy dependence is square for the breakdown strength rather than one as for the dielectric constant. For this reason, polymers, such as biaxial-oriented polypropylene (BOPP), are the primary dielectric materials currently used in dielectric capacitors due to their high E (>700 MV/m) and low dielectric loss ($<0.02\%$) [5]. However, the dielectric constants of most organic polymers are <10 in the range around 2. Because of the organic nature of polymer, the application temperature of polymer capacitors is low, which also limits their applications in high temperatures and many severe environments. While the inorganic materials, such as $BaTiO_3$, $Ba_xSr_{1-x}TiO_3$, and $PbZrTiO_3$, possess large dielectric constants and excellent heat resistance [3, 6]. Hence, inorganic dielectric materials with high dielectric constant and breakdown strength have attracted pronounced attention for high electric energy storage application.

It is a dream for material scientists to endow materials self-repairing behavior upon any damage like biological living creatures. Self-repairing behavior of materials such as

✉ Manwen Yao
yaomw@tongji.edu.cn

[1] Functional Materials Research Laboratory, School of Materials Science and Engineering, Tongji University, No. 4800 Caoan Road, Shanghai 201804, China

self-repairing concrete, self-repairing polymer and so on, achieved limited but inspiring success. For dielectric materials, aluminum electrolytic capacitor is an excellent and very successful example. Within its entire service life, any damage and defect of the alumina dielectric layer formed on the surface of aluminum foil (served as the anode of the capacitor) by anodic oxidation can be in situ mended and repaired by supplementary anodic oxidation reaction under high working electric field. The self-repairing mechanism endows the alumina dielectric layer very high breakdown strength close to its intrinsic value, which makes the electrolytic capacitors major circuit components of electronic circuit and system. However, to ensure the anodic oxidation reaction of the self-repairing process, appropriate wet electrolyte (served as the cathode of electrolytic capacitor) is very important, which may cause a lot of problems in construction of the capacitor and reliability issues. It is reasonable to consider, if it is possible to adapt the self-repairing idea to enhance the breakdown strength of thin and thick ceramic films to develop complete solid state monolithic ceramic capacitor for high-density energy storage applications.

Alumina (Al_2O_3) is an excellent dielectric material because of its unique properties, such as high breakdown strength (200–1000 MV/m), relative dielectric constant (7–10), band gap (≈ 9 eV), thermal and chemical stability, thermal conductivity, hardness and low leakage current [7–10]. Al_2O_3 ceramics are widely used as substrate and packaging material of integrated circuits, high temperature and corrosive resistant microwave and optical window and coating material in electronics and microelectronics [11, 12]. Al_2O_3 thin films in nanometer thickness can be used as gate dielectric of MOSFET of integrated circuits, while thin films in micrometer thickness are quite reasonable and promising to develop high density energy storage capacitors. Al_2O_3 thin films can be prepared by many techniques, including chemical vapor deposition (CVD), spray pyrolysis, pulsed laser deposition (PLD), magnetron sputtering, atomic layer deposition (ALD), molecular beam epitaxy (MBE), and sol–gel [8–10]. Among these approaches, the advantages of sol–gel technique are quite evident. The films can be deposited at room temperature under ambient atmosphere. There is no need to use complicated equipment under vacuum or exotic gas environment. Most importantly, doping and chemical composition of the film can be easily and accurately manipulated. Dense and highly uniform thin films in composition and phase structure can be easily derived from sol–gel process.

Furthermore, recent contributions shown that the dielectric properties of the amorphous Al_2O_3 thin films depend strongly on doping elements such as silicon [8], magnesium [13], titanium [14] and yttrium [15]. Typically, silicon is a glass forming element which is able to promote the forming of glass network structure. Titanium incorporated into the glass network structure is beneficial for connecting the broken bonds of the network, and further enhances the structural stability. Meanwhile, titanium is one of the valve metal elements which can be anodized under electric field similar to the anodic oxidation of aluminum. It is expected that the combination doping of silicon and titanium is able to improve the dielectric behavior of amorphous Al_2O_3 film. FESEM, DSC, FT-IR and XPS were performed to determine the structural characteristics of the Si–Ti co-doped Al_2O_3 films. Current–voltage and frequency-dependent dielectric constant and dielectric loss measurements were performed to reveal the dielectric properties of the films. Our findings suggest that the sol–gel deposited amorphous Si–Ti co-doped Al_2O_3 thin films have a potential application in electrical energy storage devices.

2 Experimental procedure

Al_2O_3 and $(Al_{1-0.02-x}Si_{0.02}Ti_x)_2O_y$ (x = 0.2, 0.9 and 2%) thin films represented as Al_2O_3, AST0.2, AST0.9 and AST2, respectively, were prepared by the sol–gel and spin coating technology. Firstly, aluminum isopropoxide and 50 ml glycol ether were mixed together and stirred for 30 min at 60 °C. Next, tetraethyl orthosilicate and tetrabutyl titanate were sequentially doped. Then, 0.02 mol acetylacetone acting as chelating agent was added to control the rate of hydrolysis at 70 °C under stirring. After stirring for 30 min, the solution was catalyzed with 10 ml acetic acid at 80 °C. The mixture was stirred for another 30 min and then cooled down slowly to the room temperature to get a transparent and homogeneous sol.

Before spin coating deposition of the films, the substrates ($Pt/Ti/SiO_2/Si$) were ultrasonically cleaned in acetone, deionized water and ethyl alcohol for 10 min, successively. Then the substrates were dried by blowing N_2. The thin films were deposited by spin-coating process with a spin speed of 3000 rpm for 20 s for each layer on the substrates. After each coating layer, the films were preheated at 150, 300 and 450 °C for 5 min in sequence to form solid films by evaporating the solvents and burning out the organic residues. After coating 7 layers, all of the samples were annealed at 450 °C in a muffle furnace for 3 h with a heating rate of 3 °C/min and then cooled down to room temperature slowly. To measure the electrical properties of the films, Au top electrodes with diameter of 1 mm were deposited via a shadow mask on the top of the films to form MIM (metal–insulator–metal) structure with Pt as bottom electrode.

3 Results

3.1 Structural analysis

The surface morphology of undoped and Si–Ti co-doped Al_2O_3 thin films is shown in Fig. 1. There is no apparent difference in the surface morphology of all the films. The surfaces of all the films annealed at 450 °C are dense and uniform, with no crystallization and macroscopic defects (e.g. cracks and holes). In other words, neither phase structure (remain amorphous) nor surface morphology is affected by Si–Ti co-doping. As displayed in Fig. 2, the thickness of the thin films measured by the cross-section FESEM images are 223, 212, 216, 216 nm for Al_2O_3, AST0.2, AST0.9 and AST2, respectively.

The thermal decomposition characteristics of Al_2O_3, AST0.2, AST0.9 and AST2 xerogel are illustrated in Fig. 3. To insure that the films are amorphous and the organics are completely decomposed, the heat-treated temperature of all the thin films is chosen as 450 °C [8]. The crystalline peak observed about 770 °C belongs to the titanium dioxide, where the peaks get more and more apparent with the increase of the titanium content. About 900 °C, the crystallization temperature of the amorphous Al_2O_3 increases with the addition of Si and Ti. The reason is that Si is a network-forming element, which is able to form the glass network structure locally and enhance the stability [8]. Simultaneously, titanium as a glass network intermediate element, can either join the network structure playing the role of connecting networks or enter the vacant sites of the loosely packed amorphous structure and strengthen its stability.

For clarification of the chemical state of Si and Ti in the co-doped Al_2O_3 thin films, Fig. 4 shows the FT-IR spectra of the undoped and co-doped Al_2O_3 thin films. It can be observed that there is a broad absorption band below 1000 cm^{-1} in the spectra, which is typical of the vibrations of Al_2O_3 [16]. A more and more apparent vibration absorption peak can be seen at 680 cm^{-1} with the increase of titanium content, which is attributed to Al–O–Ti vibration [17]. In addition, peaks about 900 and 1000 cm^{-1} correspond to Al–O–Al and Al–O–Si, respectively [18, 19]. According to the results, Si and Ti can replace Al and involve in the construction of the structure of Al_2O_3 film, resulting that the crystallization temperature of the amorphous Al_2O_3 increases with the addition of Si and Ti, which is consistent with the DSC analysis. Besides, compared with the other film samples, a relatively strong intensity peak between 600 and 1000 cm^{-1} can be observed in the AST0.9 film, as

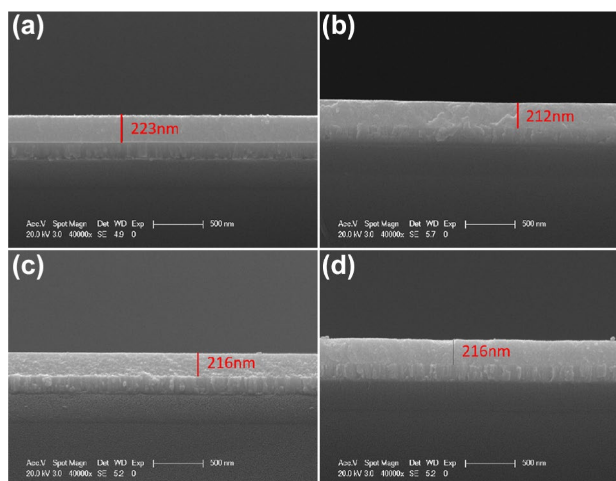

Fig. 2 Cross-section FESEM images of Al_2O_3 (**a**), AST0.2 (**b**), AST0.9 (**c**) and AST2 (**d**) thin films

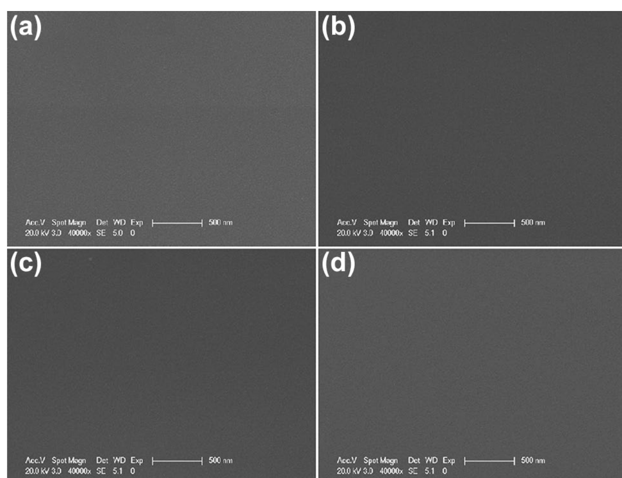

Fig. 1 Surface FESEM images of Al_2O_3 (**a**), AST0.2 (**b**), AST0.9 (**c**), and AST2 (**d**) thin films

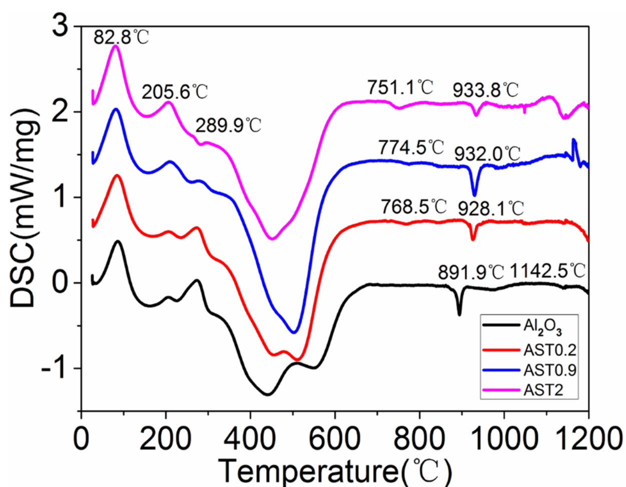

Fig. 3 DSC curves of the Al_2O_3, AST0.2, AST0.9 and AST2 xerogel

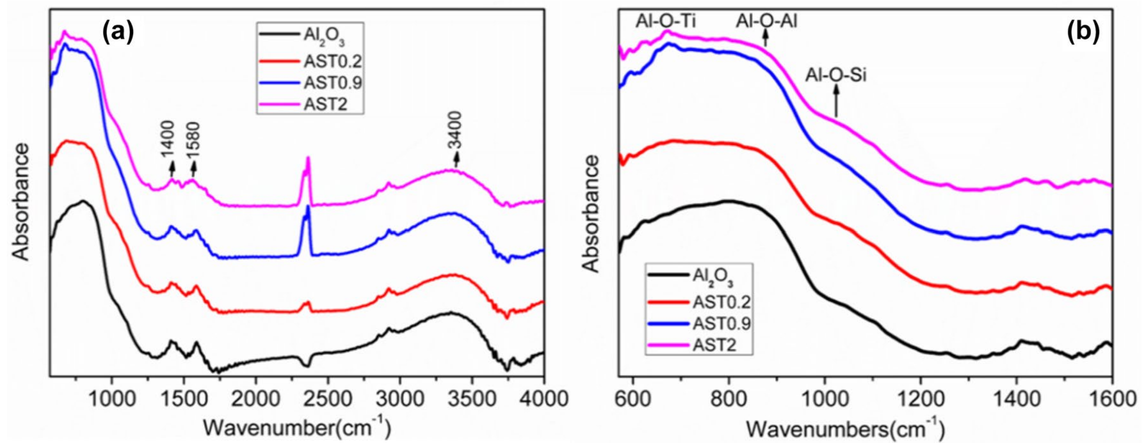

Fig. 4 FT-IR spectra of the Al_2O_3, AST0.2, AST0.9 and AST2 thin films (**a**); the partial spectra from 600 to 1600 cm^{-1} (**b**)

indicates that this co-doped component makes the Al_2O_3 film structure relatively higher stability.

The XPS survey spectra of Al_2O_3, AST0.2, AST0.9 and AST2 thin films are illustrated in Fig. 5a. As can be seen, Si and Ti elements exist in the co-doped films. The presence of C1s peak is observed due to the presence of organic residue and contaminant carbon in the air-exposed films, which can be used as an index to regulate the XPS data. To further explore the bonding state of Si and Ti in the co-doped thin films, a high resolution XPS scan was performed to explore the O1s spectrum of the AST0.9 film, as shown in Fig. 5b. The O1s peak could be curve-fitted into four components at approximately 530.01, 530.92, 531.83 and 532.61 eV, which correspond to Al–O–Ti, Al–O–Al, Al–O–Si and H_2O, successively [20, 21]. The results further confirm that the existing forms of Si and Ti in the co-doped films are Al–O–Si and Al–O–Ti, which are well agreement with the FT-IR results.

Figure 6a shows the comprehensive comparison of Ti2p spectra for the co-doped films. Clearly, both the $Ti2p_{1/2}$ and $Ti2p_{3/2}$ peaks intensity increase as the Ti doping content increases. And the binding energy about 458.6 eV of $Ti2p_{3/2}$ corresponds to Ti–O bond [22], which indicates that the more Ti content are added, the more Ti–O bond can be formed. Titanium ions are accepted to exist in films in two valence states, named as the trivalent (Ti^{3+}) and the tetravalent (Ti^{4+}) forms [22]. In order to characterize the valence state of the titanium element, high-resolution Ti2p XPS spectra of AST0.2, AST0.9 and AST2 are shown in Fig. 6b–d. As can be seen from $Ti2p_{3/2}$ peaks fitting, Ti^{4+} peak at 458.6 eV is slightly lower than total $Ti2p_{3/2}$ peak position, and a weak peak about 456 eV is revealed, which is attributed to Ti^{3+}. Based on the integral calculation of the peak areas, the $[Ti^{3+}]/[Ti]$ ratios are 27.96, 21.53 and 7.31% for AST0.2 (Ti-0.2%), AST0.9 (Ti-0.9%) and AST2

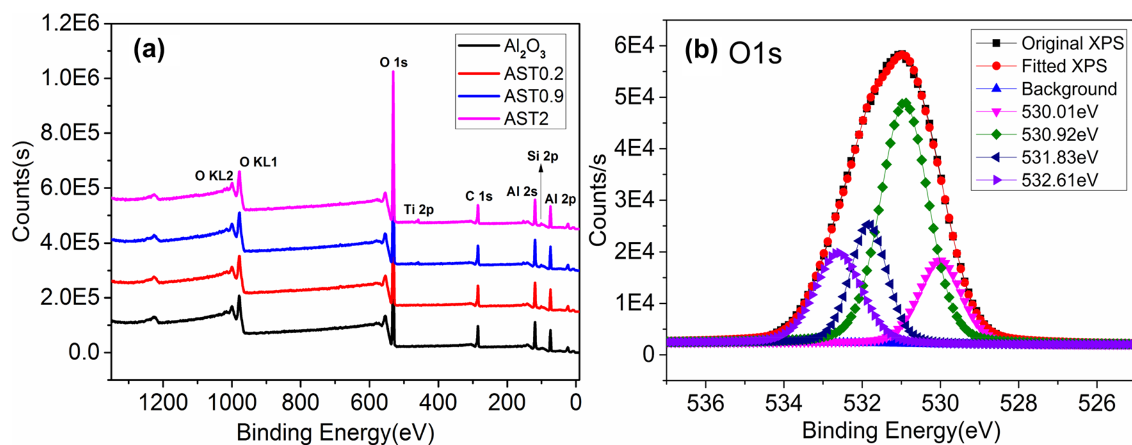

Fig. 5 XPS survey spectra of the Al_2O_3, AST0.2, AST0.9 and AST2 thin films (**a**); high-resolution XPS spectrum of O1s for the AST0.9 thin film (**b**)

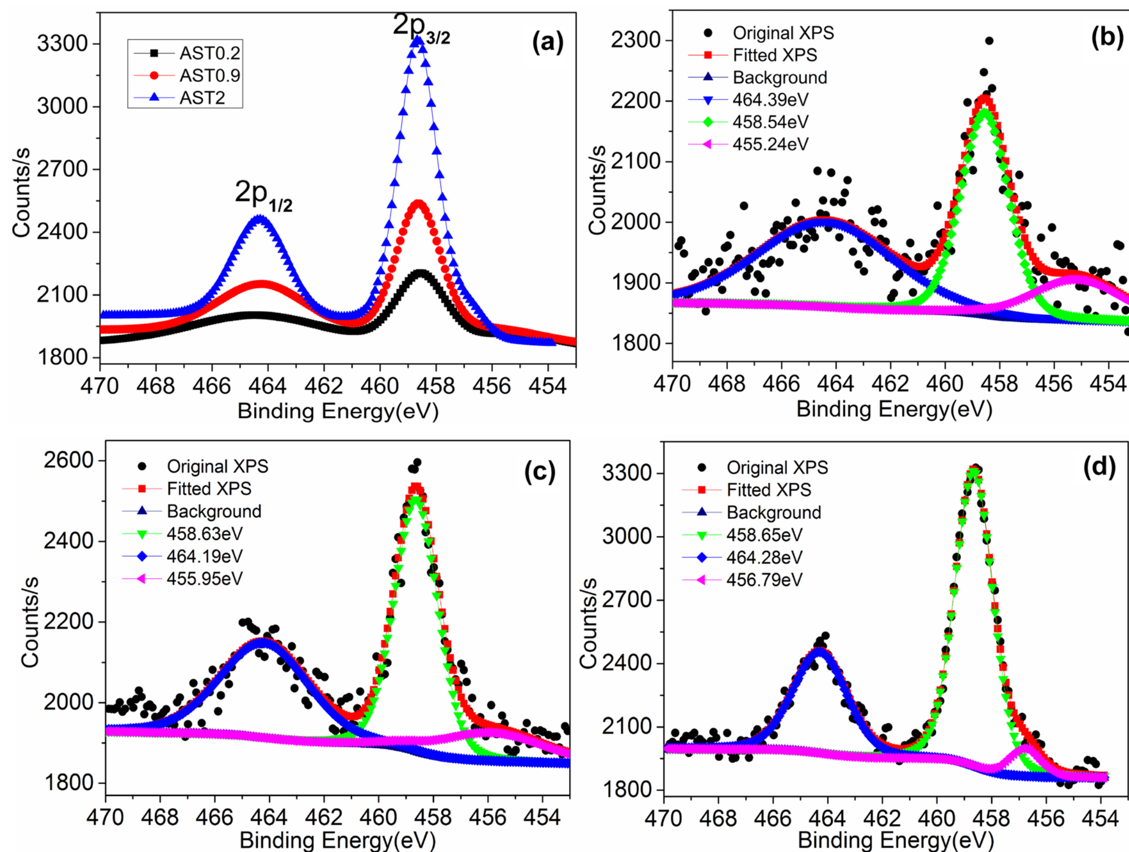

Fig. 6 High-resolution XPS spectra of Ti2p (**a**); fitted curves of Ti2p for the AST0.2 (**b**), AST0.9 (**c**) and AST2 (**d**)

(Ti-2%), respectively. And thus the $[Ti^{3+}]/[Ti+Si+Al]$ ratios are 0.05, 0.19 and 0.14%, respectively. It suggests that the AST0.9 film has the most Ti^{3+} content compared to the others.

3.2 Dielectric properties

The breakdown strength, which has an exponential influence on the energy storage capacity, is critical metric of dielectric materials. The dielectric breakdown characteristics of the Al_2O_3 and $(Al_{1-0.02-x}Si_{0.02}Ti_x)_2O_y$ thin films at room temperature are shown in Fig. 7. With the increasing of Ti content, the leakage current decreases evidently, and the breakdown voltage increases substantially. The AST0.9 thin film exhibits the lowest leakage current (from $\approx 10^{-3}$ A for Al_2O_3 film to $\approx 10^{-6}$ A for AST0.9 film) and the highest breakdown voltage (from ≈ 57 V for Al_2O_3 film to ≈ 140 V for AST0.9 film). Additionally, the leakage current increases rapidly in the low voltage region (< 30 V), while it increases slightly at higher electric field (> 30 V) until the hard breakdown. And as the voltage increases, soft breakdown occurs along with slight fluctuation of the current. The on-set voltage of the soft breakdown for the Si–Ti co-doped films is much higher than that of undoped Al_2O_3 films. The surface morphologies after hard breakdown show that the soft breakdown preferentially occurs at the electrode edge because of the edge effect [23]. In addition, there are more pinholes caused by soft breakdown for undoped Al_2O_3 films compared with the co-doped films. Especially, the AST0.9 films hardly undergoes soft breakdown at the electrode edge before the hard breakdown. It is worth noting that the holes make the Au electrode films isolate from the soft breakdown points so that the films can still keep well insulating property until the hard breakdown occurs.

In order to obtain more reliable breakdown results and exclude the influence of different thickness of various films, the Weibull distribution has been used to analysis the breakdown strength variation as shown in Fig. 8 ($E = U/d$, where U is breakdown voltage and d is thickness of films) [13–15]. As can be seen, the breakdown strength increases with the addition of Si and Ti content, especially for the AST0.9 (Ti-0.9%) films which exhibit the significantly highest breakdown strength (647 MV/m). The influence of AST0.2 (Ti-0.2%) on dielectric breakdown strength is not distinct, while it is an enhancement of 392 and 181 MV/m over that of Al_2O_3 (255 MV/m) for AST0.9 (Ti-0.9%) and AST2 (Ti-2%), respectively. It can be concluded that the Si–Ti co-doping is capable to dramatically enhance the

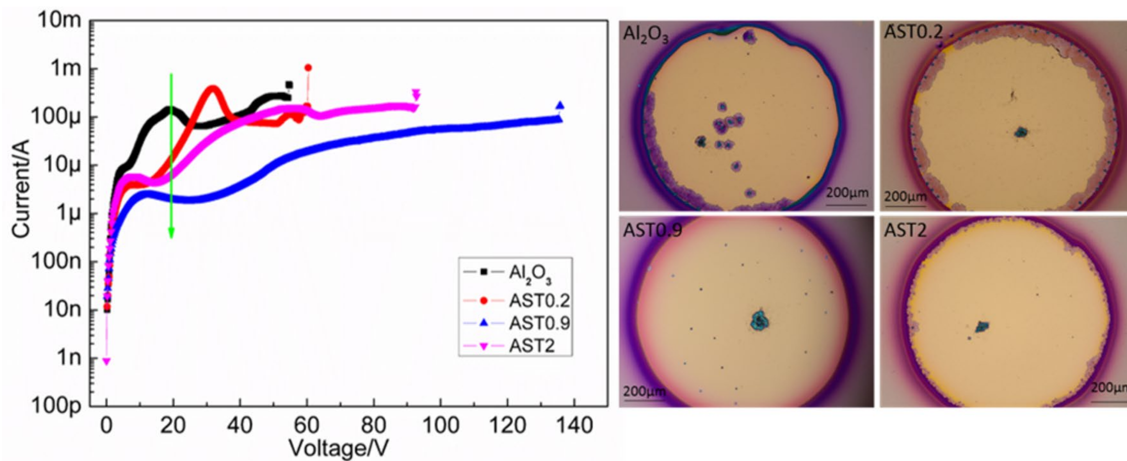

Fig. 7 Plot of I–V and metallographic photograph for the Al_2O_3 and $(Al_{1-0.02-x}Si_{0.02}Ti_x)_2O_y$ thin films

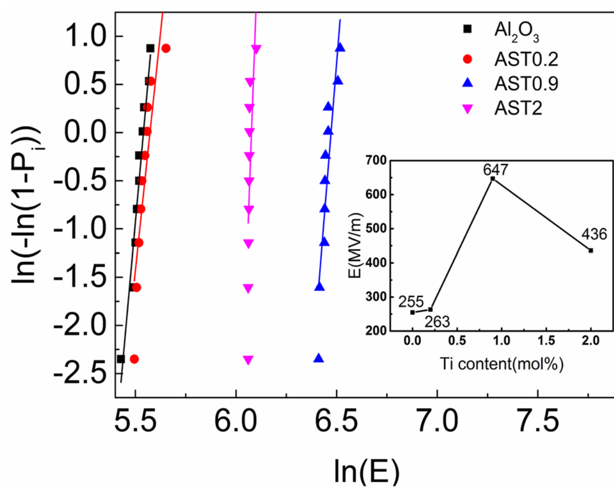

Fig. 8 Weibull distribution of the breakdown strength of the Al_2O_3 and $(Al_{1-0.02-x}Si_{0.02}Ti_x)_2O_y$ thin films. Inset shows the dependence of breakdown strength on Ti molar fraction of samples (P_i is the cumulative failure probability and E is the average breakdown strength)

breakdown strength and effectively reduce leakage current of the amorphous Al_2O_3 thin film, especially for AST0.9 (Si-2%, Ti-0.9%). The above results are consistent with the FT-IR and XPS spectra analysis, meaning that incorporation of Si and Ti into the Al_2O_3 films can strengthen the stability of the films structure thus enhance the dielectric properties.

Figure 9a–c presents the frequency-dependent dielectric constant and dielectric loss of the Al_2O_3 and Si–Ti co-doped films at room temperature. Both the dielectric constant and dielectric loss of the co-doped films are always lower than undoped Al_2O_3 films. And AST0.9 film has the lowest dielectric constant (7.56) and dielectric loss (0.02) at 100 kHz. The results are coincident with the dielectric breakdown characteristics discussed above including breakdown strength and leakage current. The amorphous Al_2O_3 thin film is linear dielectric, its theoretical energy storage density can be calculated by the formula $U_e = 1/2\varepsilon_0\varepsilon_r E^2$. The calculated values are 2.75, 2.84, 14.01 and 6.99 J/cm^3 for Al_2O_3, AST0.2, AST0.9 and AST2 thin films, respectively, as shown in Fig. 9d. Although the AST0.9 and AST2 films exhibit little lower dielectric constants (as shown in Fig. 9c), their much higher E is more crucial for the energy density obtained in these co-doped films. The energy storage density is increased by about 410 and 154% for AST0.9 and AST2 respectively in comparison with the undoped Al_2O_3 film. Some dielectric properties of the samples are shown in Table 1. The AST0.9 thin film exhibits the highest energy density due to the largest breakdown strength and relatively high dielectric constant.

4 Discussion

From the above investigations, the improvement of the dielectric strength of the Si–Ti co-doped Al_2O_3 thin films can be ascribed to the following structure modification effect of the Si–Ti co-doping. Firstly, it is well known that the radii of Si^{4+} (0.4 Å) is slightly smaller than Al^{3+} (0.535 Å), in contrast, Ti^{4+} (0.605 Å) is a little bit larger. And Si^{4+} as a kind of glass forming cation and Ti^{4+} as a network intermediate cation are introduced into the amorphous Al_2O_3 film substituting for Al^{3+} and consequently participating in the construction of the structure as shown in FT-IR and O1s XPS results. Hence, the structure of the Al_2O_3 film could become more compact and stable resulting in the improvement of the dielectric properties by Si–Ti co-doping.

From the viewpoint of defect chemistry, the concentration of oxygen vacancies ($V_O^{\cdot\cdot}$) and hydroxy anions (OH_O') of the sol–gel derived amorphous Al_2O_3 films are always

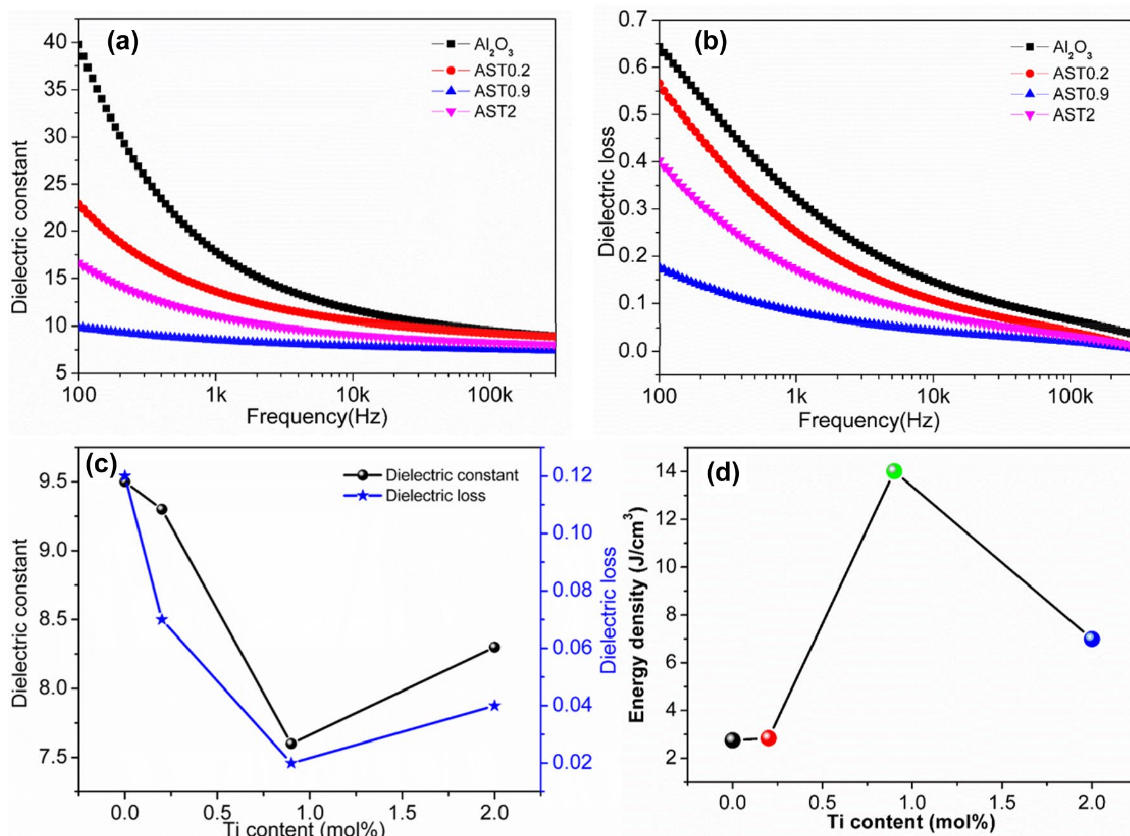

Fig. 9 Frequency dependence of dielectric constant and dielectric loss (**a–c**) at room temperature for the amorphous Al_2O_3 and $(Al_{1-0.02-x}Si_{0.02}Ti_x)_2O_y$ thin films; the dependence of energy density on Ti molar fraction of the samples (**d**)

Table 1 Some properties of Al_2O_3 and Si–Ti co-doped Al_2O_3 thin films (where J is the leakage current density when the voltage is 20 V and tanδ and ε_r are the dielectric loss and dielectric constant respectively when the frequence is 100 kHz)

Samples	U_e (J/cm^3)	E (MV/m)	J (A/cm^2)	tanδ	ε_r
Al_2O_3	2.75	255	10^{-2}	0.12	9.54
AST0.2	2.84	263	10^{-3}	0.07	9.28
AST0.9	14.01	647	10^{-4}	0.02	7.56
AST2	6.99	436	10^{-4}	0.04	8.31

high. They can be regarded as the major intrinsic defects of the film. Since both defects are positive charged, hence, they are able to capture electrons and serve as electron traps [24]. The trapped electron can be again detrapped from their hosts under various high electric field and eventually initiate a local breakdown event at the defect region [25]. If the breakdown energy is high enough to demolish the insulation behavior of the sample, then such breakdown is regarded as a hard breakdown, otherwise, the recoverable breakdown events can be regarded as soft breakdowns. Usually, for dielectric films there are lots of soft breakdown events taking place ahead of the final hard breakdown under various electric field. Whereas, according to the defect chemistry, Si and Ti doping in alumina film can be described as follow:

$$3SiO_2 \xrightarrow{2Al_2O_3} 3Si_{Al}^{\cdot} + 6O_O + V_{Al}^{\prime\prime\prime}$$

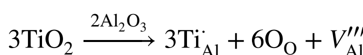

$$3TiO_2 \xrightarrow{2Al_2O_3} 3Ti_{Al}^{\cdot} + 6O_O + V_{Al}^{\prime\prime\prime}$$

The above defect reaction equations reveal that the cation vacancies ($V_{Al}^{\prime\prime\prime}$) can be generated by Si and Ti doping, which are able to effectively suppress the formation of oxygen vacancies ($V_O^{\cdot\cdot}$) and thus reduce the traps density in the Al_2O_3 film. Therefore, the Si–Ti co-doped Al_2O_3 thin films exhibit much higher structural stability and breakdown strength in comparison with undoped Al_2O_3 film. And the combination of the two intrinsic defects is counted as a defect associate which has no net charge and thus has no contribution to the conductivity [15]. The generation of defect associates by Si and Ti co-doping could results in lower leakage current and dielectric loss.

Besides, in general, the local energy around the defects is always higher than that of the normal state. There is a tendency for the distorted structure region with higher

energy to be minimized to restore back to its normal structure [8, 12]. Simultaneously, the difference of the ionic radius and the micro pores originated from the thermal decomposition of the organic groups can provide the ionic migration channels and promote the ionic migration in the amorphous thin films. As a consequence, the appropriate ions can be transported to the location of the defects under the applied electric field and combined with each other to repair the defects, block the channels and thus improve the breakdown strength. Especially, the Ti2p XPS results imply that the AST0.9 (Si-2%, Ti-0.9%) film has the most Ti^{3+} content compared with the other components, which can be anodized to Ti^{4+}. The reaction is described as:

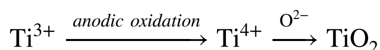

$$Ti^{3+} \xrightarrow{anodic\ oxidation} Ti^{4+} \xrightarrow{O^{2-}} TiO_2$$

The dense TiO_2 formed by anodic oxidation can effectively prevent the breakdown and play the role of self-repairing. As a result, the AST0.9 film with the most Ti^{3+} content exhibits the strongest self-repairing capability (performing the highest breakdown strength and the lowest leakage current and dielectric loss).

5 Conclusion

The dense and uniform amorphous Al_2O_3 and Si–Ti co-doped Al_2O_3 thin films were deposited on Pt/Ti/SiO_2/Si substrates using sol–gel technology. The FT-IR and XPS results revealed that Si and Ti occupied Al site in the films, existing in the form of Al–O–Si and Al–O–Ti, involving in the construction of the Al_2O_3 structure and strengthening the structural stability. The high-resolution Ti2p XPS further reveals that Ti^{3+} existed in the co-doped films and the self-repairing capability (anodic oxidation) is enhanced with the increasing of the Ti^{3+} content. The co-doped films exhibit significantly enhanced breakdown strength and energy storage density as well as relatively low leakage current and dielectric loss, particularly for the AST0.9 (Si-2%, Ti-0.9%) film. And the $(Al_{0.971}Si_{0.02}Ti_{0.009})_2O_y$ thin films exhibits the ultrahigh energy density of 14.01 J/cm^3 under the breakdown strength of 647 MV/m, which is 410% over the Al_2O_3 thin films (2.75 J/cm^3 at 255 MV/m). The results suggest that Si–Ti co-doped Al_2O_3 thin films have perspective dielectric properties and self-repairing capability for use in electric energy storage devices.

Acknowledgements This work is supported by the National Natural Science Foundation of China (Grant No. 61761136004) and the Ministry of Science and Technology of China through 973-project (Grant No. 2015CB654601).

Compliance with ethical standards

Conflict of interest The authors declare that they have no conflict of interest.

References

1. C. Liu, F. Li, L. Ma, H. Cheng, Advanced materials for energy storage. Adv. Mater. **22**, 28–62 (2010)
2. Z. Xie, Z. Yue, B. Peng, J. Zhang, C. Zhao, X. Zhang, G. Ruehl, L. Li, Large enhancement of the recoverable energy storage density and piezoelectric response in relaxor-ferroelectric capacitors by utilizing the seeding layers engineering. Appl. Phys. Lett. **106**, 202901 (2015)
3. Y. Wang, J. Cui, Q. Yuan, Y. Niu, Y. Bai, H. Wang, Significantly enhanced breakdown strength and energy density in sandwich-structured barium titanate/poly(vinylidene fluoride) nanocomposites. Adv. Mater. **27**, 6658–6663 (2015)
4. H. Zhu, Z. Liu, F. Wang (2017) Improved dielectric properties and energy storage density of poly(vinylidene fluoride-cotrifluoroethylene-co-chlorotrifluoroethylene) composite films with aromatic polythiourea. J. Mater. Sci. https://doi.org/10.1007/s10853-016-0742-6
5. X. Zhang, Y. Shen, B. Xu, Q. Zhang, L. Gu, J. Jiang, J. Ma, Y. Lin, C.W. Nan, Giant energy density and improved discharge efficiency of solution-processed polymer nanocomposites for dielectric energy storage. Adv. Mater. **28**, 2055–2061 (2016)
6. Q.K. Muhammad, M. Waqar, M.A. Rafiq, Structural, dielectric, and impedance study of ZnO-doped barium zirconium titanate (BZT) ceramics. J. Mater. Sci. **51**, 1–11 (2016). https://doi.org/10.1007/s10853-016-0231-y
7. Z. Su, M. Yao, F. Li, Y. Peng, Q. Feng, X. Yao (2017) Microstructural transitions and dielectric properties of boron-doped amorphous alumina thin film. J. Mater. Sci. https://doi.org/10.1007/s10853-017-1127-1
8. M. Yao, Z. Su, P. Zou, J. Chen, F. Li, Q. Feng, X. Yao, Dielectric properties under high electric field for silicon doped alumina thin film with glass-like structure derived from sol-gel process. J. Alloys Compd. **690**, 249–255 (2017)
9. A.B. Khatibani, S.M. Rozati, Growth and molarity effects on properties of alumina thin films obtained by spray pyrolysis. Mater. Sci. Semicond. Process. **18**, 80–87 (2014)
10. P. Katiyar, C. Jin, R.J. Narayan, Electrical properties of amorphous aluminum oxide thin films. Acta Mater. **53**, 2617–2622 (2005)
11. Z. Pan, J. Zhai, B. Shen, Multilayer hierarchical interfaces with high energy density in polymer nanocomposites composed of $BaTiO_3$@TiO_2@Al_2O_3 nanofibers. J. Mater. Chem. A **5**, 15217–15226 (2017)
12. M. Yao, Y. Peng, R. Xiao, Q. Li, X. Yao, Enhanced self-repairing capability of sol-gel derived $SrTiO_3$/nano Al_2O_3 composite films. Appl. Phys. Lett. **109**, 092904 (2016)
13. Y. Peng, M. Yao, R. Xiao, X. Yao, Electrical properties of sol-gel derived Mg-doped Al_2O_3 films. J. Mater. Sci. Mater. Electron. **27**, 11495–11501 (2016)
14. M. Yao, R. Xiao, Y. Peng, J. Chen, B. Hu, X. Yao, The influence of titanium doping on the electric properties of amorphous alumina films prepared by sol-gel technology. J. Sol-Gel. Sci. Technol. **74**, 39–44 (2015)
15. M. Yao, P. Zou, Z. Su, J. Chen, X. Yao, The influence of yttrium on leakage current and dielectric properties of amorphous Al_2O_3 thin film derived by sol-gel. J Mater Sci Mater Electron **27**, 7788–7794 (2016)

16. P.K. Sharma, M.H. Jilavi, D. Burgard, R. Nass, H. Schmidt, Hydrothermal synthesis of nanosize α-Al_2O_3 from seeded aluminum hydroxide. J. Am. Ceram. Soc. **81**, 2732–2734 (1998)
17. V.A. Zeitler, C.A. Brown, The infrared spectra of some Ti-O-Si, Ti-O-Ti and Si-O-Si compounds. J. Phys. Chem. C **61**, 1174–1177 (1957)
18. L. Stoch, M. Środa, Infrared spectroscopy in the investigation of oxide glasses structure. J. Mol. Struct. **511–512**, 77–84 (1999)
19. T.M.H. Costa, M.R. Gallas, E.V. Benvenutti, J.A.H. Jornada, Study of nanocrystalline γ-Al_2O_3 produced by high-pressure compaction. J. Phys. Chem. B **103**, 4278–4284 (1999)
20. NIST X-ray photoelectron spectroscopy database (2012), http://srdata.nist.gov/xps/
21. S. Seal, A. Kale, K.B. Sundaram, D. Jimenez, Oxidation and chemical state analysis of polycrystalline magnetron sputtered (Ti, Al)N films at ambient and liquid N_2 temperatures. J. Vac. Sci. Technol. A **18**, 1571 (2000)
22. F.H. ElBatal, M.A. Marzouk, H.A. ElBatal, Optical and crystallization studies of titanium dioxide doped sodium and potassium silicate glasses. J. Mol. Struct. **1121**, 54–59 (2016)
23. M. Yao, J. Chen, Z. Su, Y. Peng, P. Zou, X. Yao, Anodic oxidation in aluminum electrode by using hydrated amorphous aluminum oxide film as solid electrolyte under high electric field. ACS Appl. Mater. Interfaces **8**, 11100–11107 (2016)
24. D. Liu, S.J. Clark, J. Robertson, Oxygen vacancy levels and electron transport in Al_2O_3. Appl. Phys. Lett. **96**, 032905 (2010)
25. K. Ganesan, S. Ilango, M. Shanmugam, M.F. Baroughi, M. Kamruddin, A.K. Tyagi, Pre- and post-breakdown electrical studies in ultrathin Al_2O_3 films by conductive atomic force microscopy. Curr. Appl. Phys. **13**, 1865–1869 (2013)